Optics and Laser Technology 122 (2020) 105830

Contents lists available at ScienceDirect

Optics and Laser Technology

journal homepage: www.elsevier.com/locate/optlastec

Full length article

Automated segmentation of fluid regions in optical coherence tomography B-scan images of age-related macular degeneration

Zailiang Chen[a,b], Dabao Li[a,b], Hailan Shen[a,*], Hailan Mo[a,b], Ziyang Zeng[a,b], Hao Wei[a,b]

[a] School of Computer Science and Engineering, Central South University, Changsha 410083, China
[b] Hunan Engineering Research Center of Machine Vision and Intelligent Medicine, Changsha 410083, China

HIGHLIGHTS

- The fluid region can be automatically segment by integrating SE blocks with U-Net structure.
- This method can effectively improve the segmentation results compared with U-Net and SegNet.
- We present effective pre-processing to reduce the false positive rate of segmentation results.
- This work can classify OCT B-scan to AMD OCT and normal OCT images based on segmentation results.

ARTICLE INFO

Keywords:
SEUNet
AMD
OCT image
Fluid regions
Segmentation

ABSTRACT

Age-related macular degeneration (AMD) is a common eye disease that causes progressive vision loss in people older than 50 years. Fluid regions in retina are the most characteristic of AMD. Accurately segmenting fluid regions is crucial for the early diagnosis of AMD, and assessment of treatment efficacy. In this paper, we propose an automatic deep learning method constructed by integrating Squeeze-and-Excitation blocks with U-Net named SEUNet to segment fluid regions and classify OCT B-scan images to AMD or normal image. The proposed method comprises three stages: (1) preprocessing stage that includes image noise removal, locating the image on the area of interest, and image color-reversing; (2) fluid region segmentation stage which is based on U-Net and constructed by integrating Squeeze-and-Excitation block to segment fluid region; and (3) image classification stage that classifies image to AMD or normal image. Experimental results show that the proposed method have an average IOU coefficient of 0.9035, an average Dice coefficient of 0.9421, an average precision of 0.9446, and an average recall of 0.9464. Therefore, the proposed method can effectively segment fluid regions in OCT B-scan images.

1. Introduction

Age-related macular degeneration (AMD) is a common eye disease that causes progressive degeneration of the central vision in many countries [1] and is a complex retinal disease that develops from a combination of risk factors such as environment, lifestyle and genetics are great. This illness causes vision loss due to abnormal blood vessel growth through Bruch's membrane (BM) thus leading to fluid leakage into the retina [1]. Fluid regions in retina are one of the characteristic of AMD [2]. Their size and location are vital biomarkers for AMD progression [3].

Optical coherence tomography (OCT) has been widely used to diagnose eye diseases, such as glaucoma [4], AMD, diabetic macular edema (DME), anemia screening [5], and to visualize retinal structures such as retinal layer [6], exudates, and retinal fluid regions [7]. Therefore, detection and quantitative assessment of retinal fluid regions are facilitated by OCT B-scan images. An example of fluid regions in OCT B-scan image is shown in Fig. 1. Fluid regions are restricted to the layers between the inner limiting membrane (ILM) and BM. Accurately segmenting fluid regions is crucial for the early diagnosis of AMD, and assessment of treatment efficacy [8]. Manually segmenting fluid regions from each OCT B-scan image by an experienced ophthalmologist is difficult, labor-intensive, and time-consuming, especially if these regions are small [9]. The segmentation results are non-reproducible and subjective. Therefore, an accurate semi-automatic or automatic fluid regions segmentation method is highly sought.

* Corresponding author.
E-mail addresses: xxxyczl@163.com (Z. Chen), lidabao@csu.edu.cn (D. Li), hn_shl@126.com (H. Shen), xiaomianhua@csu.edu.cn (H. Mo), zengziyang@csu.edu.cn (Z. Zeng), csuweihao@csu.edu.cn (H. Wei).

https://doi.org/10.1016/j.optlastec.2019.105830
Received 28 January 2019; Received in revised form 9 July 2019; Accepted 6 September 2019

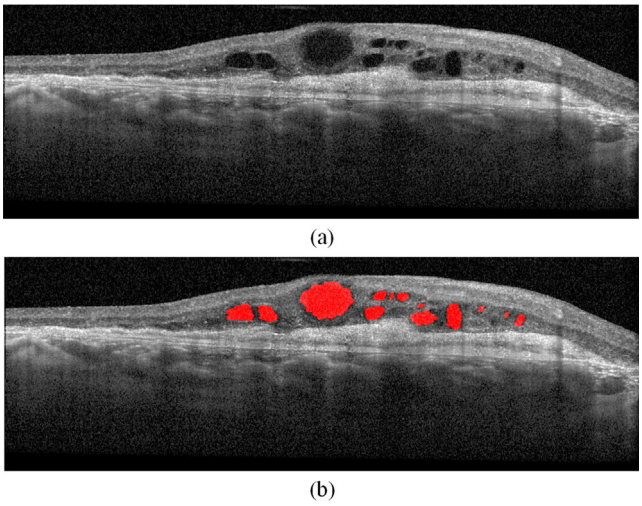

Fig. 1. Example of OCT B-scan showing fluid regions. (a) An OCT B-scan image. (b) Manually segmentation of fluid regions in red. (For interpretation of the references to color in this figure legend, the reader is referred to the web version of this article.)

For the past decades, different approaches have been proposed to effectively segment fluid regions from OCT B-scan image. These methods can be divided into three categories. (1) Graph-based methods [10–12]. Those methods use graph cut to segment fluid regions. Each OCT image can be represented as a weighted graph, each pixel corresponds to anode, and the neighboring nodes are connected by weighted edges. Two additional nodes, namely source and sink, are added to represent fluid region and background, respectively. Each node in the graph is connected to source and sink with a weighted edge. Finally, the fluid regions are segmented by minimizing the energy function of the graph cut. These methods have high computational burden, and are sensitive to the specific of fluid region and background seed points. (2) Traditional learning-based methods [13–16]. In these methods, a classifier is trained based on feature extraction to classify each pixel to fluid region or background. For each sample point, a set of features, such as textural, structural, and positional information, is calculated before the training stage. After feature extraction, dimensionality reduction and feature selection are used to improve the accuracy of the classifier. During testing, the same set of features is extracted for each pixel. Each pixel is then classified to fluid region or background using the trained classifier. In these methods, a large number of features must be calculated to improve the accuracy of the segmentation results, thereby increasing the computational burden and memory burden. These methods cannot achieve high accuracy of segmentation results because they limited by the feature extraction. (3) Deep learning-based methods [7,9,17,18]. Fully convolutional network (FCN) [19] has made tremendous breakthroughs for biomedical image segmentation. These methods use FCN structure, such as U-Net [20] and SegNet [21], to segment fluid regions. FCN can accept input OCT images of any size and use the convolutional layer to extract feature map. The deconvolution layer is utilized to upsample the feature map of the last convolutional layer and restore its size similar to that of the input OCT image to generate a prediction for each pixel. The spatial information in the original input OCT image is preserved, and per-pixel classification is finally performed on the upsampled feature map.

In this work, we propose a method to segment fluid regions in OCT B-scan image, and classify OCT B-scan to AMD or normal images. The proposed method is based on FCN, where fluid regions is segmented through the semantic segmentation of the OCT B-scan image. Our method is constructed by integrating SE-blocks in SENet [22] with U-Net, termed as SEUNet, to segment fluid regions on OCT image. This paper has three main contributions. First, we propose a method that can automatically segment fluid region by integrating SE-blocks with U-Net structure. This method can effectively improve the segmentation results compared with U-Net and SegNet. Second, we present effective preprocessing through image denoising, retinal layer segmentation, and extraction of the region of interest (ROI) and image color-reversing to reduce the false positive rate of segmentation results. Third, this work can classify OCT B-scan to AMD OCT and normal OCT images based on segmentation results.

2. Methods

The proposed method is designed to automatically segment fluid region and classify OCT images which is shown in Fig. 2. The proposed method comprises three stages: (1) preprocessing stage that includes image noise removal, tracking of the image on the region of interest and image color-reversing; (2) fluid region segmentation stage that can automatically segment fluid region; and (3) image classification stage that classify images to AMD or normal images.

2.1. Preprocessing

In this study, we perform preprocessing for the OCT image from three aspects: (1) BM3D denoising, (2) retinal layer segmentation, and (3) extraction of the ROI and image color-reversing.

According to the special imaging principle of OCT images, which is based on coherent detection, speckle noise [23] is the main source of noise in OCT images. Speckle noise is the reason for the random distribution of the image pixel amplitude, and the resulting granular distribution structure blurs the fine features of the image, which is not conducive to medical diagnosis. Hence, BM3D algorithm [24] is used on each OCT image to remove speckle noise. This algorithm is a block-matching denoising method using sparse 3D transform-domain collaborative filtering. The denoising process suppresses OCT speckle noise while sharpening the image to improve the presentation of fluid region.

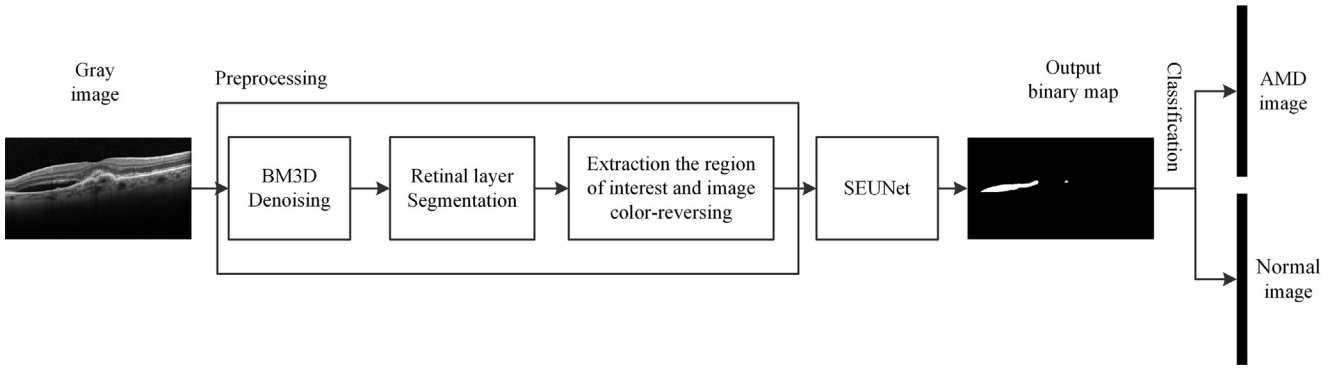

Fig. 2. Block diagram of the proposed method.

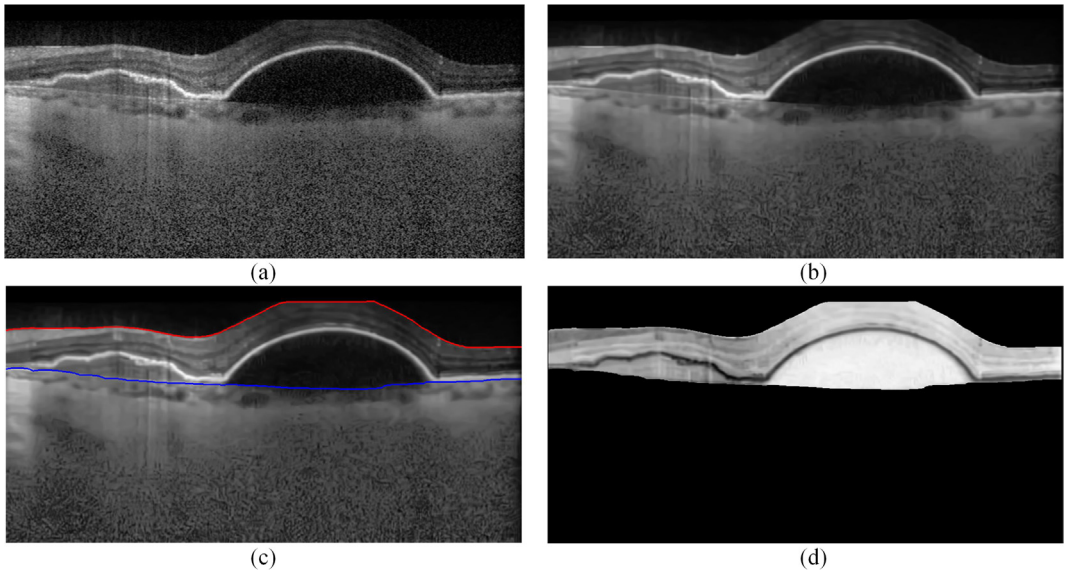

Fig. 3. Sketch map of preprocessing stage. (a) OCT B-scan image. (b) Image after denoising. (c) Retinal layer segmentation. (d) ROI and image color-reversing. (For interpretation of the references to colour in this figure legend, the reader is referred to the web version of this article.)

The denoising result is shown in Fig. 3(b). After the image denoising process, the retinal region is segmented from denoised OCT image. Fluid region is restricted to the layers between ILM and BM, the first and last retinal layers on the retinal region, respectively. And fluid regions are known to be restricted to the layers between ILM and BM. Extraction ROI of retinal can improve the segmentation of fluid regions. Various segmentation algorithms have been proposed for segmenting retinal layers. The layer segmentation methods are based on our previous work [25] which is proposed for segment OCT image with AMD. We modify this graph-based segmentation approach to suitably segment retinal layers. The retinal layer segmentation results are shown in Fig. 3(c). After retinal layer segmentation, ROI can be extracted, and image color-reversing is implemented on the ROI. The ROI is shown in Fig. 3(d).

2.2. Fluid region segmentation

For the fluid region segmentation stage, we propose a method which is based on U-Net and is constructed by integrating Squeeze-and-Excitation block (SE-block) with U-Net, to segment fluid regions on OCT B-scan images. SE-block automatically acquires the degree of importance of each feature map, and then enhances the feature maps that are useful and suppresses the useless feature maps according to the degree of importance. SE-block mainly consists of three parts, namely, squeeze, excitation and scale. The SE-block structure is illustrated in Fig. 4. The squeeze operation is the global average pooling operation in SE-block, as shown in Eq. (1).

$$u_c = F_{sq}(x_c) = \frac{1}{H \times W} \sum_{i}^{H} \sum_{j}^{W} x_c(i, j) \tag{1}$$

where u_c is the c-th element of the squeezed feature map, $F_{sq}(\cdot)$ is the squeeze operation, x_c is the c-th feature map of the input, and H and W are the height and width of the input tensor, respectively.

In the subsequent excitation operation, the weights of feature maps from input tensor are delineated. This operation is the fully connected operation in SE-block, and is shown in Eq. (2).

$$v_c = F_{ex}(u_c) = \sigma(W_2(\delta(W_1(u_c)))) \tag{2}$$

where v_c is the output vector of the weights of feature maps, $F_{ex}(\cdot)$ is the excitation operation, σ(·) is ReLU activation function, δ(·) is Sigmoid activation function, and W_1 and W_2 denote the fully connected operation.

Finally, the scale operation rescales the input tensor according to the output vector of the weights of feature maps. as shown in Eq. (3).

$$y_c = F_{scale}(v_c) = v_c * u_c \tag{3}$$

where y_c is the output of SE-block and $F_{scale}(\cdot)$ is the excitation operation.

The proposed SEUNet architecture is illustrated in Fig. 5. In the original U-Net, we replace each convolution layer by SE-block. The architecture consists of a contracting path and an expanding path. The former is used to obtain context information, and the latter is used for

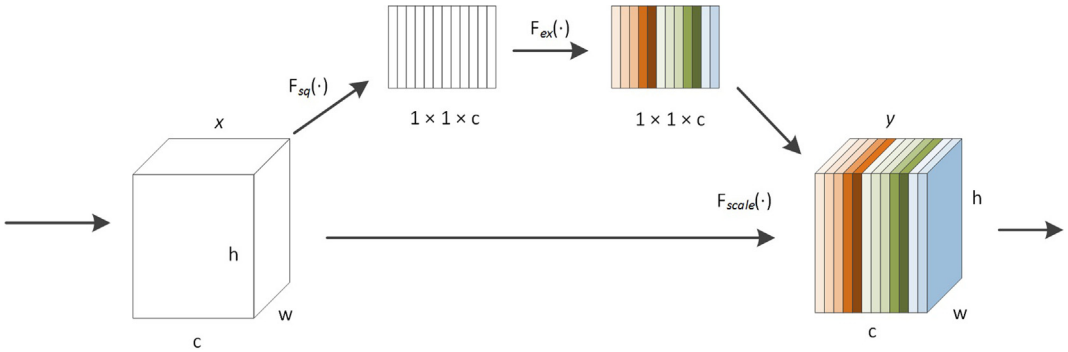

Fig. 4. Squeeze-and-Excitation block.

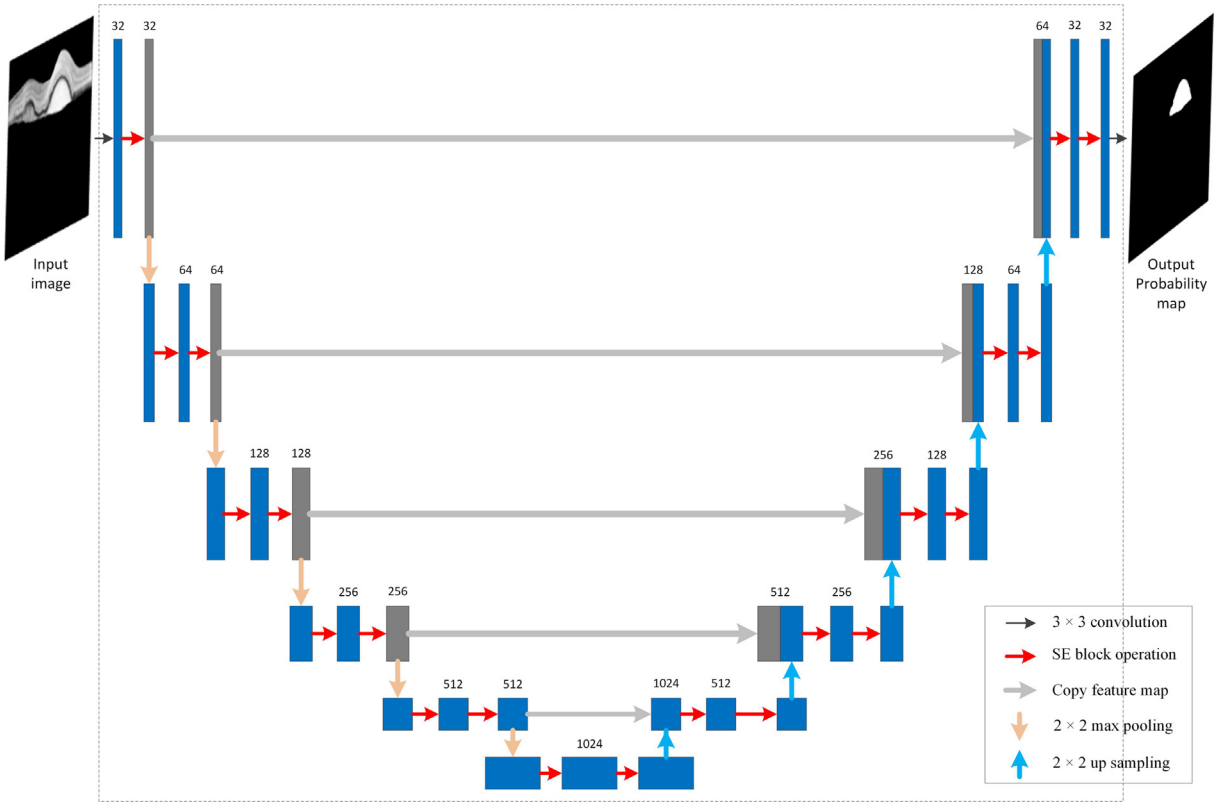

Fig. 5. Proposed SEUNet architecture for depth = 5.

precise localization information. The two paths are symmetric with each other. The proposed method can obtain precise context information and localization information by integrating SE-block with U-Net.

The loss function in our SEUNet is the Dice loss shown Eqs. (4) and (5)

$$l(A, B) = -\log d(A, B) \tag{4}$$

$$d(A, B) = \frac{2\sum_{i=1}^{\bar{H}}\sum_{j=1}^{\bar{W}}(a_{i,j}b_{i,j})}{\sum_{i=1}^{\bar{H}}\sum_{j=1}^{\bar{W}}(a_{i,j})^2\sum_{i=1}^{\bar{H}}\sum_{j=1}^{\bar{W}}(b_{i,j})^2} \tag{5}$$

where A is the predicted output map, $a_{i,j} \in \{0, 1\}$ is pixel value at point (i, j) in A, B is the actual binary output map, $b_{i,j} \in \{0, 1\}$ is pixel value at point (i, j) in B, and $\bar{H}$ and $\bar{W}$ are the height and width of the input image, respectively.

2.3. Image classification

After segmentation of fluid regions, the OCT B-scan images can be classified into AMD and normal images. The classification is to illustrate the superiority of our segmentation results since AMD patients with small fluid regions are able to segmented and classified. During testing, the predicted output map can be obtained by the SEUNet. If all pixels of the predicted output map belong to the background, then the OCT B-scan image can be classified into normal image. Otherwise, even if only one pixel is detected as fluid region, this B-scan will be classified as AMD. As shown in Fig. 6, the predicted output map of Fig. 6(a) has pixels belonging to fluid regions. Hence, Fig. 6(a) can be classified into AMD image. On the contrary the pixels of the predicted output map of Fig. 6(b) belong to the background and thus can be classified into normal image.

3. Results and discussions

3.1. Datasets

A publicly available dataset by Rashno et al. [10] is used for the experiments to evaluate the performance of the proposed method. This dataset consists of 600 OCT B-scans from 24 AMD patients and is randomly split into 450 training images and 150 testing images. All of the B-scans images are captured by the Heidelberg Spectralis imaging device, and obtained by averaging 12–19 frames with a resolution of 5.88 μm/pixel along the length and 3.87 μm/pixel along the width. The fluid regions are manually segmented by two experienced ophthalmologists from the University of Minnesota. Inter-observer Dice coefficient and intersection-over-Union (IOU) coefficient for the fluid region segmentation results on all OCT images of two experienced ophthalmologists are calculated as 0.894 and 0.869, respectively. For result evaluation, using the average of experienced ophthalmologist's manual segmentation results for train and test the proposed network.

The training data only contained 450 OCT images which are not abundant to train the SEUNet. Therefore, data augmentation is used to generate sufficient training data. The training data are increased by random translation, reflection, rotation, flipping and cropping. After data augmentation, the total number of training data is increased to 13,500 OCT images.

3.2. Evaluation

The following four performance metrics are used to evaluate the accuracy of fluid region segmentation as follows: IOU coefficient, Dice coefficient, precision, recall. $IOU(A, B) = \left|\frac{A \cap B}{A \cup B}\right|$ and $Dice(A, B) = \frac{2\,|A \cap B|}{|A| + |B|}$ are used to quantitatively evaluate the similarity between segmentation results and corresponding ground truth. $precision = \frac{|A \cap B|}{|A|}$ and $recall = \frac{|A \cap B|}{|B|}$ are used to measure the correct segmentation, where A is the segmentation result, B is the ground truth.

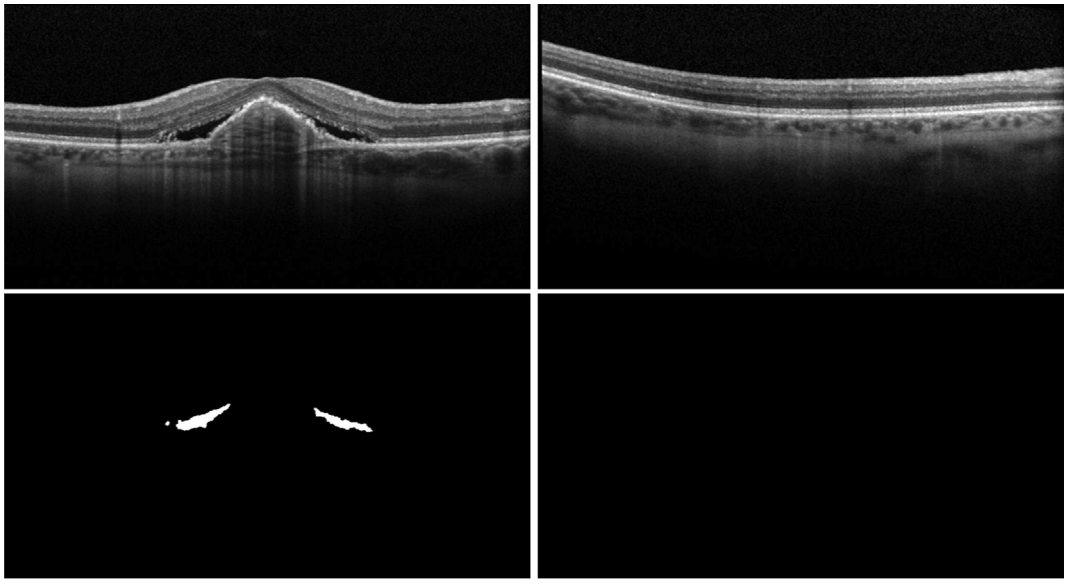

Fig. 6. Image classification. The first row is B-scan images, and the second row is predicted output maps. (a) OCT B-scan image is belonging to AMD image. (b) OCT B-scan image is classified into normal image.

Three performance metrics are used to evaluate the accuracy of OCT image classification as follows: $precision = \frac{TP}{TP+FP}$, $recall = \frac{TP}{TP+FN}$ and $accuracy = \frac{TP+TN}{TP+FP+FN+TN}$, where *TP* is the number of correctly classified as positive, *TN* is the number of correctly classified as negative, *FP* is the number of wrongly classified as positive, and *FN* is the number of wrongly classified as negative.

3.3. Results

The depth of the proposed SEUNet architecture affects the segmentation results. If the depth is too small or large, then the proposed SEUNet method cannot learn the complex features from training OCT images. This phenomenon causes SEUNet overfitting or underfitting, which reduces the segmentation accuracy. Table 1 shows that the proposed SEUNet can achieve best segmentation results when the depth is 5. Hence, the depth of proposed SEUNet architecture is set as 5.

Fluid regions segmentation results of the proposed method are compared with the ground truth, kernel graph cut in neutrosophic domain (KGCNE) [10], U-Net [20], SegNet [21], SegNet with SE-block. Those methods all use the same preprocessing and loss function. The fluid region segmentation results of four cases from the 150 test OCT images. Our proposed method has been evaluated with respect to IOU coefficient, Dice coefficient, precision and recall criteria. The IOU coefficient, Dice coefficient, precision and recall are shown in Table 2, and the best results are in bold from. As shown in Table 2, our method achieves an IOU coefficient of 0.9035, a Dice coefficient of 0.9421, precision of 0.9446 and recall of 0.9494. The segmentation results of our method show improvements by average of 3.3%, 2.8%, 0.06%, and 1.4% on the IOU coefficient, Dice coefficient, precision and recall, respectively, when compared with those of KGCNE, U-Net, SegNet and SegNet with SE-block Those results indicated that the proposed algorithm can effectively segment fluid regions in OCT B-scan images.

Table 1
Evaluation of the segmentation results for vary depth of ours SEUNet.

	Depth = 3	Depth = 4	Depth = 5	Depth = 6
IOU	0.8471	0.8983	**0.9031**	0.8985
Dice	0.8962	0.8777	**0.9418**	0.9384
Parameters	0.26M	1.05M	4.21M	16.81M

Table 2
Evaluation of the segmentation results for test OCT image compare with those of KGCNE, U-Net, SegNet and SegNet method.

	KGCNE [10]	U-Net [20]	SegNet [21]	SegNet with SE-block	Our method (depth = 5)
IOU	0.7828	0.8594	0.8542	0.8742	**0.9035**
Dice	0.8576	0.9028	0.9037	0.9157	**0.9421**
precision	0.9249	0.9440	0.9195	0.9290	**0.9446**
recall	0.8321	0.9012	0.9238	0.9354	**0.9494**

The qualitative are shown in Fig. 7. The first row is the ground truth, and the second to fifth rows are the segmentation results of KGCNE, U-Net, SegNet, SegNet with SE-block and our methods. Column 1 shows a simple case, in which the fluid region differs from the normal tissue. The five segmentation methods expect SegNet show good perform-ance. Column 2 is a case where the fluid regions are similar to the normal tissues. Under-segmentation of the fluid regions is evident in the results of KGCNE and U-Net. Column 3 is a case wherein the part fluid regions are small. In this case, KGCNE and U-Net methods cannot correctly segment the fluid regions. Column 4 is a case in which the OCT B-scan is a normal OCT image, and U-Net has wrongly segmented the fluid regions. Therefore, the proposed method performs better than KGCNE, U-Net, SegNet, and SegNet with SE-block for the segmentation of fluid regions.

As shown in Table 3, the SEUNet show improvements of 27.3%, 22.8%, 15.1%, and 11.1% in the IOU coefficient, Dice coefficient, precision and recall, respectively, when compared with SEUNet-WP. The accuracy of our SEUNet without denoising and our SEUNet without ROI extraction also have improved. Fig. 8 illustrates the fluid region segmentation results of our SEUNet compared with our SEUNet without preprocessing (SEUNet-WP), our SEUNet without denoising and our SEUNet without ROI extraction. The cases in first row are the ground truths, the second row are the SEUNet-WP's results, the third row are the values of our SEUNet without denoising, the fourth row are the the values of SEUNet without ROI extraction and the fifth row are the our SEUNet's values. For the first cases in column 1, the fluid region segmentation of our SEUNet-WP and our SEUNet without ROI extraction

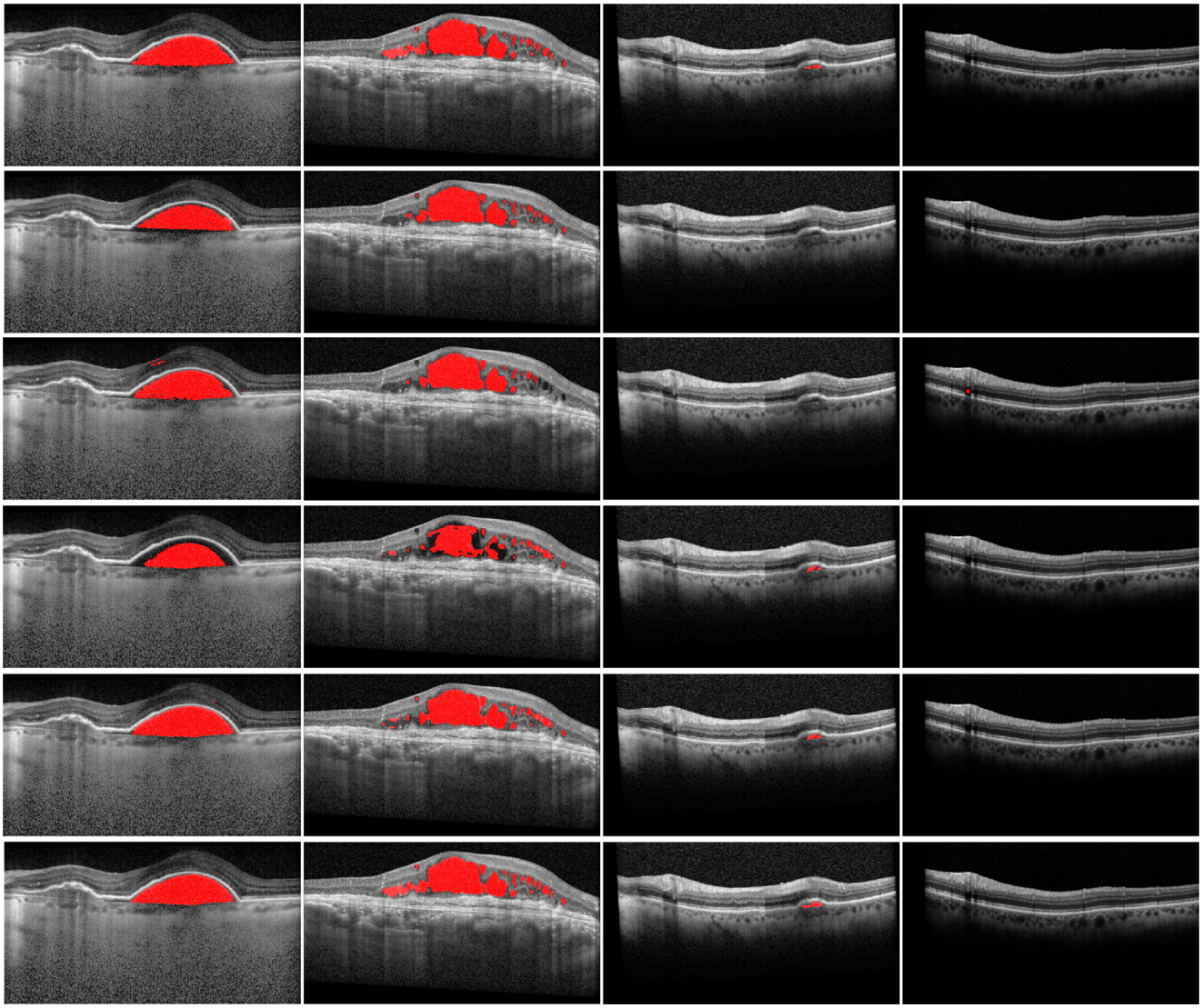

Fig. 7. Fluid regions segmentation results from different methods. Column 1 to 4 are different cases. The first to sixth rows are the segmentation results of ground truth, KGCNE, U-Net, SegNet, SegNet with SE-block and SEUNet methods, respectively.

has failed. The regions segmented by SEUNet-WP and SEUNet without ROI extraction are found in Choroid under BM. Fluid regions are restricted to the layers between ILM and BM, hence, this result is error. Our SEUNet with preprocessing can ignore the regions above ILM and under BM. The results of our SEUNet without ROI extraction are more badly, because some Choroid regions are similar to fluid regions after the denoising steps. For the second case in column 2, the SEUNet-WP and SEUNet without ROI extraction method cannot segment fluid regions. For the third case, under-segmentation of the fluid regions is evident in the segmentation results of SEUNet-WP and SEUNet without ROI extraction. While, the segmentation results of our SEUNet without denoising have some unsegmented points. This unsegmented point is noise point in fluid regions. The results indicate that the preprocessing method plays an important role in our segmentation pipeline.

In order to verify the effectiveness of the SEUNet, Our SEUNet can classify OCT B-scan images into normal and AMD images. The predicted output map can be obtained by the SEUNet. If all pixels of the predicted output map belong to the background, then the OCT B-scan image is classified into normal image. Otherwise, even if only one pixel is detected as fluid region, this B-scan will be classified as AMD. The image classification results for 150 test OCT images are shown in Table 4. The numbers of OCT B-scan images misclassified by KGCNE, U-Net, SegNet, and SEUNet-WP are 5, 4, 4, and 7, respectively. In our SEUNet, one normal image is classified into AMD image, all AMD images are

Table 3
Evaluation of the segmentation results for test OCT image compare with our SEUNet-WP, our SEUNet without denoising and our SEUNet without ROI extraction method.

	Our SEUNet-WP (depth = 5)	Our SEUNet without denoising (depth = 5)	Our SEUNet without ROI extraction (depth = 5)	Our SEUNet (depth = 5)
IOU	0.7095	0.8948	0.7127	**0.9035**
Dice	0.7670	0.9221	0.7761	**0.9421**
precision	0.8210	0.9260	0.8353	**0.9446**
recall	0.8543	0.9323	0.8605	**0.9494**

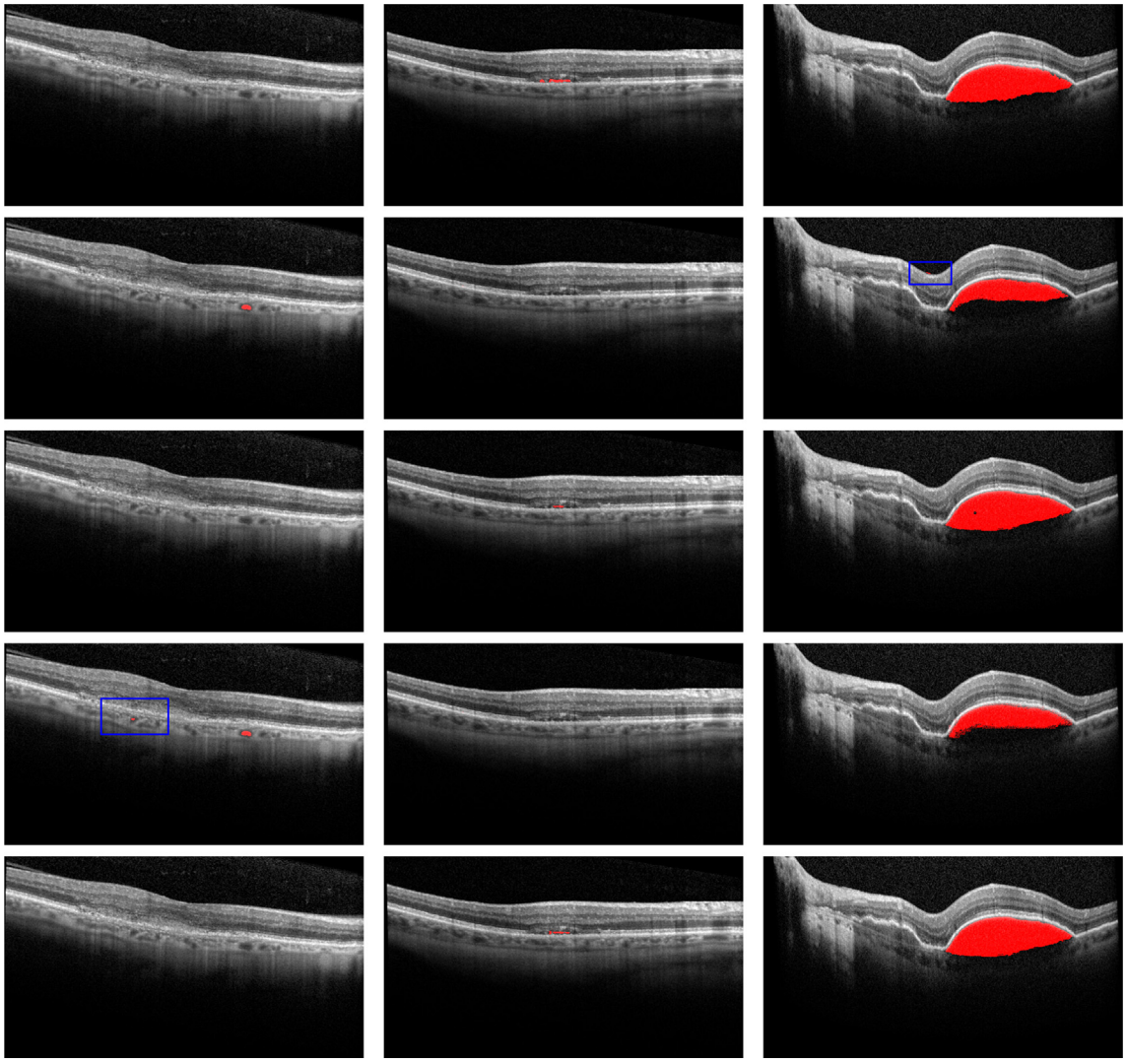

Fig. 8. Fluid regions segmentation results of our methods. Column 1 to 3 are different cases. The first to fifth rows are the segmentation results of ground truth, our SEUNet-WP, our SEUNet without denoising, our SEUNet without ROI extraction and our SEUNet method.

Table 4
The image classification results of the 150 test OCT images.

	precision	recall	accuracy
KGCNE [10]	0.967	0.977	0.967
U-Net [20]	0.977	0.977	0.973
SegNet [21]	0.967	0.988	0.973
SegNet with SE-block	0.977	0.988	0.98
SEUNet-WP (depth = 5)	0.946	0.977	0.953
SEUNet (depth = 5)	**0.989**	**1**	**0.993**

classified correctly. The results of classification indicate that our SEUNet method can classify OCT B-scan images into normal and AMD image.

4. Conclusions

In this paper, a method constructed by integrating SE-blocks with U-Net (termed as SEUNet) is proposed for segmentation of fluid regions in OCT images. The proposed method comprises three stages: (1) pre-processing stage that includes image noise removal, tracking of the image on the region of interest and image color-reversing; (2) fluid region segmentation stage that can automatically segment fluid region; and (3) image classification stage that classify images to AMD or normal images. The segmentation results show that the proposed SEUNet has an average IOU coefficient of 0.9035, an average Dice coefficient of 0.9421, an average precision of 0.9446, and an average recall of 0.9494. The classification results show that the proposed SEUNet has an average precision of 0.989, an average recall of 1, and an average accuracy of 0.993. Compared with KGCNE, U-Net, SegNet, SegNet with SE-block, and SEUNet-WP, our proposed method achieved the state-of-the-art performance in this public dataset for the segmentation of OCT images. Moreover, we proved the effectiveness of SE-Block in the segmentation task in this paper, especially for the OCT image segmentation. Finally, our method provided a powerful pipeline for fluid segmentation, which plays an important role in ophthalmic disease assisted diagnosis in future. In future work, we will continue to adding more effective network structure to improve the performance of our network and we will extend the proposed method to segment of fluid regions in OCT B-scan images of other kinds of eye diseases, such as diabetic macular oedema, and central serous retinopathy.

Acknowledgements

This research was supported by the National Natural Science Foundation of China, China, under Grant No. 61672542 and supported by the Fundamental Research Funds for the Central Universities of

Central South University, China, under Grant No. 2018zzts566.

References

[1] L.S. Lim, P. Mitchell, J.M. Seddon, F.G. Holz, T.Y. Wong, Age-related macular degeneration, Lancet 379 (9827) (2012) 1728–1738.

[2] M.W. Wintergerst, T. Schultz, J. Birtel, A.K. Schuster, N. Pfeiffer, S. Schmitz-Valckenberg, F.G. Holz, R.P. Finger, 'Algorithms for the automated analysis of age-related macular degeneration biomarkers on optical coherence tomography: a systematic review', Translational Vision Sci. Technol. 6 (4) (2017) 10.

[3] S.G. Zadeh, M.W. Wintergerst, V. Wiens, S. Thiele, F.G. Holz, R.P. Finger, T. Schultz, CNNs enable accurate and fast segment-ation of drusen in optical coherence tomography: deep learning in medical image analysis and multimodal learning for clinical decision support, Springer, 2017, pp. 65–73.

[4] T. Khalil, M.U. Akram, H. Raja, A. Jameel, I. Basit, Detection of glaucoma using cup to disc ratio from spectral domain optical coherence tomography images, IEEE Access 6 (2018) 4560–4576.

[5] Z. Chen, Y. Mo, P. Ouyang, H. Shen, D. Li, R. Zhao, Retinal vessel optical coher-ence tomography images for anemia screening, Med. Biol. Eng. Compu. (2018) 1–14.

[6] R. Poddar, J.S. Werner, Implement-ations of three OCT angiography (OCTA) methods with 1.7 MHz A-scan rate OCT system on imaging of human retinal and choroidal vasculature, Opt. Laser Technol. 102 (2018) 130–139.

[7] G.N. Girish, B. Thakur, S.R. Chowdhury, A.R. Kothari, J. Rajan, Segmentation of intra-retinal cysts from optical coherence tomography images using a fully convolutional neural network model, IEEE J. Biomed. Health. Inf. 23 (1) (2018) 296–304.

[8] S.M. Waldstein, J. Wright, J. Warburton, P. Margaron, C. Simader, U. Schmidt-Erfurth, Predictive value of retinal morphology for visual acuity outcomes of different ranibizumab treatment regimens for neovascular AMD, Ophthalmology 123 (1) (2016) 60–69.

[9] F.G. Venhuizen, B.G. Van, B. Liefers, F.A. Van, V. Schreur, S. Fauser, C. Hoyng, T. Theelen, C.I. Sánchez, Deep learning approach for the detection and quantification of intraretinal cystoid fluid in multivendor optical coherence tomography, Biomed. Opt. Exp. 9 (4) (2018) 1545–1569.

[10] A. Rashno, B. Nazari, D.D. Koozekanani, P.M. Drayna, S. Sadri, H. Rabbani, K.K. Parhi, Fully-automated segmentation of fluid regions in exudative age-related macular degeneration subjects: Kernel graph cut in neutrosophic domain, PLoS ONE 12 (10) (2017) e0186949.

[11] A. Rashno, D.D. Koozekanani, P.M. Drayna, B. Nazari, S. Sadri, H. Rabbani, K.K. Parhi, Fully-automated segmentation of fluid/ cyst regions in optical coherence tomography images with diabetic macular edema using neutrosophic sets and graph algorithms, IEEE Trans. Biomed. Eng. 65 (5) (2018) 989–1001.

[12] H. Bogunović, M.D. Abràmoff, M. Sonka, Geodesic graph cut based retinal fluid segmentation in optical coherence tomography, Proceedings of the Ophthalmic Medical Image Analysis, 2015, pp. 49–56.

[13] L. Zhang, W. Zhu, F. Shi, H. Chen, X. Chen, Automated segmentation of intra-retinal cystoid macular edema for retinal 3D OCT images with macular hole, Biomedical Imaging (ISBI), 2015 IEEE 12th International Symposium on, IEEE, 2015, pp. 1494–1497.

[14] X. Xu, K. Lee, L. Zhang, M. Sonka, M.D. Abràmoff, Stratified sampling voxel classification for segmentation of intraretinal and subretinal fluid in longitudinal clinical OCT data, IEEE Trans. Med. Imaging 34 (7) (2015) 1616–1623.

[15] S.J. Chiu, M.J. Allingham, P.S. Mettu, S.W. Cousins, J.A. Izatt, S. Farsiu, Kernel regression based segmentation of optical coher-ence tomography images with diabetic macular edema, Biomed. Opt. Exp. 6 (4) (2015) 1172–1194.

[16] A. Lang, A. Carass, E.K. Swingle, O. Al-Louzi, P. Bhargava, S. Saidha, H.S. Ying, P.A. Calabresi, J.L. Prince, Automatic segmentation of microcystic macular edema in OCT, Biomed. Opt. Exp. 6 (1) (2015) 155–169.

[17] C.S. Lee, A.J. Tyring, N.P. Deruyter, Y. Wu, A. Rokem, A.Y. Lee, Deep-learning based, automated segmentation of macular edema in optical coherence tomography, Biomed. Opt. Exp. 8 (7) (2017) 3440–3448.

[18] T. Schlegl, S.M. Waldstein, H. Bogunovic, F. Endstraßer, A. Sadeghipour, A.M. Philip, D. Podkowinski, B.S. Gerendas, G. Langs, U. Schmidterfurth, Fully automated detection and quantification of macular fluid in OCT using deep learning, Ophthalmology 125 (4) (2018) 549–558.

[19] J. Long, E. Shelhamer, T. Darrell, Fully convolutional networks for semantic segmentation, Proc Proceedings of the IEEE conference on computer vision and pattern recognition, 2015, pp. 3431–3440.

[20] O. Ronneberger, P. Fischer, T. Brox, U-net: convolutional networks for biomedical image segmentation, Proc. International Confer-ence on Medical image computing and computer-assisted intervention, 2015, pp. 234–241.

[21] V. Badrinarayanan, A. Kendall, R. Cipolla, Segnet: a deep convolutional encoder-decoder architecture for image segmentation, IEEE Trans. Pattern Anal. Mach. Intell. 39 (12) (2017) 2481–2495.

[22] J. Hu, L. Shen, G. Sun, Squeeze-and-excitation networks, Proc Proceedings of the IEEE Conference on Computer Vision and Pattern Recognition, 2018, pp. 7132–7141.

[23] J.M. Schmitt, S. Xiang, K.M. Yung, Speckle in optical coherence tomography, J. Biomed. Opt. 4 (1) (1999) 95–106.

[24] K. Dabov, A. Foi, V. Katkovnik, K. Egiazarian, BM3D image denoising with shape-adaptive principal component analysis, Proc. SPARS'09-Signal Processing with Adaptive Sparse Structured Representations, 2009, pp. 1–6.

[25] Z. Chen, D. Li, H. Shen, et al., Automated retinal layer segmentation in oct images of age-related macular degeneration, IET Image Process. 13 (11) (2019) 1824–1834.